Effect of adipose tissue thickness and tissue optical properties on the differential pathlength factor estimation for NIRS studies on human skeletal muscle

ILEANA PIROVANO,[1,*] SIMONE PORCELLI,[2,3] REBECCA RE,[1,4] LORENZO SPINELLI,[4] DAVIDE CONTINI,[1] MAURO MARZORATI,[2] AND ALESSANDRO TORRICELLI[1,4]

[1]*Dipartimento di Fisica, Politecnico di Milano, Milan, Italy*
[2]*Istituto di Tecnologie Biomediche, Consiglio Nazionale delle Ricerche, Segrate, Milan, Italy*
[3]*Dipartimento di Medicina Molecolare, Università di Pavia, Pavia, Italy*
[4]*Istituto di Fotonica e Nanotecnologie, Consiglio Nazionale delle Ricerche, Milan, Italy*
[*]ileana.pirovano@polimi.it

Abstract: We propose a quantitative and systematic investigation of the differential pathlength factor (DPF) behavior for skeletal muscles and its dependence on different factors, such as the subcutaneous adipose tissue thickness (ATT), the variations of the tissue absorption (μ_a) and reduced scattering (μ'_s) coefficients, and the source-detector distance. A time domain (TD) NIRS simulation study is performed in a two-layer geometry mimicking a human skeletal muscle with an overlying adipose tissue layer. The DPF decreases when μ_a increases, while it increases when μ'_s increases. Moreover, a positive correlation between DPF and ATT is found. These results are supported by an *in-vivo* TD NIRS study on *vastus lateralis* and *biceps brachii* muscles of eleven subjects at rest, showing a high inter-subject and inter-muscle variability.

1. Introduction

Near Infra-Red Spectroscopy (NIRS) is a non-invasive technique that allows the assessment of oxidative metabolism in skeletal muscles at rest and during exercise [1–3]. The energy production during tissue activity relies mainly on oxygen (O_2) availability inside the cells, therefore, an increase in energy demand leads to an increase in oxidative metabolism and O_2 delivery from the vascular bed [4]. In fact, the O_2 bound to hemoglobin (Hb) molecules inside the red blood cells is released and diffuses towards the muscle fibers, where it can bind and be stored in the myoglobin (Mb) or utilized in the mitochondria [5]. NIRS estimates fractional O_2 extraction in skeletal muscle, by measuring the concentration of oxygenated Hb and Mb ([oxy(Hb + Mb)]) and deoxygenated Hb and Mb ([deoxy(Hb + Mb)]) in the tissue. Most of the NIRS studies on skeletal muscles reported in the literature have been conducted by using Continuous Wave (CW) NIRS. This technique only allows the estimation of variations with respect to an arbitrary baseline value of [oxy(Hb + Mb)] and [deoxy(Hb + Mb)], by measurements of light attenuation changes. If CW NIRS multi-distance measurements are performed, the tissue oxygen saturation (S_tO_2) can also be estimated [6].

The simplest approach to interpret CW NIRS data, using only one source-detector separation distance ρ, relies on the modified Lambert-Beer Law to retrieve Hb and Mb concentrations changes over the experimental time t. Under the simplifying hypothesis that the scattering in the tissue and the input intensity are constant, the light attenuation changes at wavelength λ can be

expressed as:

$$\Delta A\left(\lambda, t; t_0\right) \approx -\ln\left(\frac{I\left(\lambda, t\right)}{I\left(\lambda, t_0\right)}\right) = \sum_{i=1}^{n}\left[\epsilon_i\left(\lambda\right) \cdot \Delta C_i\left(t; t_0\right)\right] \rho DPF\left(\lambda\right) \tag{1}$$

where $I(\lambda, t)$ is the light intensity measured at the detector at time t, $I(\lambda, t_0)$ is the light intensity at the detector at the reference time t_0, $\Delta C_i(t; t_0)$ and $\varepsilon_i(\lambda)$ are the concentration change and the specific extinction coefficient of the i-th chromophore. Finally, DPF(λ) is the Differential Pathlength Factor, a dimensionless coefficient introduced to take into account that, because of scattering events, the photons pathlength in diffusive biological tissues is not equal to ρ [7].

To estimate DPF(λ), it is possible to employ Time Domain (TD) NIRS or Frequency Domain (FD) NIRS, or also a diffuse optical tomography setup for CW NIRS. In particular, with TD NIRS it is possible to measure the Distribution of Time-of-Flight (DTOF) due to the path travelled by photons inside the tissue, and it is therefore possible to directly derive the DPF as:

$$DPF\left(\lambda\right) \cong \frac{1}{\rho} \cdot \frac{c}{n\left(\lambda\right)} t\left(\lambda\right) \tag{2}$$

where c is the speed of light in vacuum, $n(\lambda)$ is the tissue refractive index at wavelength λ, and $\langle t(\lambda) \rangle$ is the photon mean time-of-flight [8].

By using a semi-infinite homogeneous model for photon diffusion, it is also possible to relate the DPF to the absorption coefficient (μ_a) and the reduced scattering coefficient (μ'_s) [9]:

$$DPF\left(\lambda\right) \approx \frac{1}{2}\sqrt{\frac{3\mu'_s\left(\lambda\right)}{\mu_a\left(\lambda\right)}}\left[1 - \frac{1}{\left(1 + \rho\sqrt{3\mu_a\left(\lambda\right)\mu'_s\left(\lambda\right)}\right)}\right]. \tag{3}$$

When CW systems with only one source-detector separation distance ρ are employed, the estimate of the DPF by Eq. (2) or Eq. (3) cannot be applied. Therefore, DPF values are usually taken from literature and kept constant in the study. However, the majority of the DPF studies reported in literature involve brain measurements [9–11]. On the other hand, data from literature concerning DPF of skeletal muscle [12,13] suggested that the values could also depend on specific characteristics of the muscle itself, the subcutaneous adipose tissue thickness (ATT) and the muscle condition *e.g.*, rest or exercise. Moreover, since DPF depends also on the measurement time, the wavelength and the tissue optical properties, keeping constant values introduces inaccuracy in the estimation of [oxy(Hb + Mb)] and [deoxy(Hb + Mb)]. Actually, it is still not completely clear how this simplifying assumption can affect the derived parameters related to muscle oxidative metabolism. Indeed, it has been reported that the DPF value can affect the magnitude of the calculated concentration changes, and since it depends on the wavelength, it can also cause cross-talk between oxy[Hb + Mb] and deoxy[Hb + Mb] estimates [14,15].

To the best of our knowledge, there is a lack of quantitative and systematic works that investigate the DPF behavior in skeletal muscle tissue and its dependence on different factors such as ρ, ATT and the variations of μ_a and μ'_s. The DPF dependence on the medium geometry and optical properties for CW photon diffusion was analytically examined by Piao *et al.* in 2015 [16]. However, they investigated only cylinder and sphere geometries as to mimic the NIRS measurement conditions on infant head and short source-detector separation, but no considerations about limbs or muscles were carried out.

In this work, we aimed at evaluating the effect of ATT and optical properties changes on the estimation of DPF in skeletal muscle. To this purpose, we first performed a TD NIRS simulation study in a two-layer geometry with varying optical properties and different ATT values; then we carried out *in-vivo* TD NIRS measurements at rest on the upper and lower limbs muscles of eleven healthy subjects.

2.　Materials and methods

2.1.　Analytical simulations

Limbs are heterogeneous and layered structures. When light is delivered to them, the principal layers encountered are the skin, the subcutaneous adipose tissue and the skeletal muscle. This architecture influences the photons optical path length and the optical properties. In order to better investigate the influence of the optical properties and the thickness of the adipose layer on photons path length, we performed an analytical simulation study. Since the skin thickness is usually very small *i.e.*, between 1 and 2 mm [17], we simplified our model considering a diffusive medium composed by only two layers: a first one comprehensive of both the skin and the subcutaneous adipose tissue and a second layer simulating the skeletal muscle. We exploited the analytical solution of the Diffusion Equation for a bilayer model [18] to simulate the time-resolved reflectance curves obtained with different combinations of μ_a, μ'_s and ATT.

Eight different values for ATT were simulated *i.e.*, 1, 2, 2.5, 5, 7.5, 10, 12.5, 15 mm, in order to cover the typical range of values found on human limbs during *in-vivo* acquisitions [19]. We identified with the subscript "0" parameters of the first layer and with subscript "1" the coefficients of the second layer *i.e.*, μ_{a0}, μ'_{s0}, μ_{a1}, μ'_{s1}. To investigate separately the effect of absorption and scattering on the DPF, only one parameter at a time was changed. In particular, for each ATT value, the μ_a and μ'_s of the first and second layer were varied alternatively. The combinations of the parameters used for the four simulations are summarized in Table 1.

Table 1. Combination of simulated optical properties for each ATT considered. In the first two simulations, only the first layer coefficients values were increased (Inc.) or decreased (Dec.), while on the other two simulations the second layer properties were tested.

	First layer coefficients	Second layer coefficients
	$\mu'_{s0} = 10 \text{ cm}^{-1}$	
Simulation 1	Inc. $\mu_{a0} = 0.15{:}0.05{:}0.6 \text{ cm}^{-1}$	
	Dec. $\mu_{a0} = 0.15{:}(\text{-}0.015){:}0.015 \text{ cm}^{-1}$	$\mu_{a1} = 0.15 \text{ cm}^{-1}$
	$\mu_{a0} = 0.05 \text{ cm}^{-1}$	$\mu'_{s1} = 8 \text{ cm}^{-1}$
Simulation 2	Inc. $\mu'_{s0} = 8{:}0.5{:}12.5 \text{ cm}^{-1}$	
	Dec. $\mu'_{s0} = 8{:}(\text{-}0.5){:}3.5 \text{ cm}^{-1}$	
		$\mu'_{s1} = 8 \text{ cm}^{-1}$
Simulation 3		Inc. $\mu_{a1} = 0.15{:}0.05{:}0.6 \text{ cm}^{-1}$
	$\mu_{a0} = 0.05 \text{ cm}^{-1}$	Dec. $\mu_{a1} = 0.15{:}(\text{-}0.015){:}0.015 \text{ cm}^{-1}$
	$\mu'_{s0} = 10 \text{ cm}^{-1}$	$\mu_{a1} = 0.15 \text{ cm}^{-1}$
Simulation 4		Inc. $\mu'_{s1} = 8{:}0.5{:}12.5 \text{ cm}^{-1}$
		Dec. $\mu'_{s1} = 8{:}(\text{-}0.5){:}3.5 \text{ cm}^{-1}$

Since the first layer was intended to mainly resemble the subcutaneous adipose tissue, which is usually less absorbing and more diffusive than muscle at the operating wavelengths of TD NIRS measurements, we initially set $\mu'_{s0} > \mu'_{s1}$ and $\mu_{a0} < \mu_{a1}$ [20,21]. Then, in order to investigate the influence of the optical property changes, a wide range of variation of the parameters was allowed from the starting point, both increasing and decreasing them. An in-house built software written in C language was used for this purpose, implementing the two-layer model for photon diffusion in the time domain [22].

For each combination of parameters, ten repeated DTOFs were generated with a fixed total number of photons equal to 10^6. The simulated digital signal was represented over 4096 channels, with a bin resolution of 3.05 ps/channel. A constant background signal of 4 photons/channel was also simulated and a noise following the Poisson distribution was added to the theoretical model.

Moreover, to take into account the non-ideality of the instrumentation, the theoretical model was convoluted with an experimental Instrument Response Function (IRF) acquired with the same device that was employed in the *in-vivo* study (described in paragraph 2.2.2).

In a previous study by Scholkmann and Wolf [23], it was stated that the DPF in the human head can depend also from the source-detector separation ρ when this is below 25 mm, while this dependence can be considered negligible for larger distances. Since we wanted to test this condition also for skeletal muscle, we simulated two source-detector separation distances just below and above this threshold: a short distance $\rho_s = 15$ mm and a long distance $\rho_L = 30$ mm.

2.2. In-vivo measurements

The aim of this part of the study was to quantitatively determine the DPF and its dependence on the tissue properties directly during *in-vivo* measurements. To achieve this goal, the *vastus lateralis* and the *biceps brachii* muscles of healthy volunteers were probed with TD NIRS technique.

2.2.1. Population description and experimental protocol

Eleven subjects participated in the study after signing an informed consent. The experiments were conducted in accordance with the Declaration of Helsinki, and the study was approved by the local Ethical Committee of ITB-CNR (#58/2019).

Subjects had an average ($\pm$ SD) age of 28.5 ± 6.8 years and a similar level of physical activity. Measurements of the subcutaneous ATT above the probed region were taken with a skin fold caliper (C10 Plicometer Tanner–Whitehouse; Holtain, Ltd., Crymych, UK) and calculated as half of the skinfold thickness. An average ($\pm$ SD) ATT of 4.1 ± 2.0 mm was measured for legs and 1.9 ± 0.4 mm for arms. In Table 2, anthropometric characteristics of the subjects are reported.

Table 2. Subjects' anthropometric characteristics: age in years, weight in kg, height in cm, leg and arm adipose tissue thicknesses in mm.

Subject's ID	Age [years]	Weight [kg]	Height [cm]	Leg ATT [mm]	Arm ATT [mm]
1	27	66.1	190	3.9	4.4
2	25	60.3	170	8.0	4.6
3	28	66.7	172	1.9	3.4
4	26	74.9	178	6.6	4.8
5	25	64.7	171	2.0	3.0
6	25	87.1	191	4.9	5.4
7	24	66.7	173	3.6	3.2
8	25	64.0	172	4.5	3.9
9	38	74.0	175	2.5	2.4
10	26	63.5	173	2.2	3.2
11	45	77.5	183	5.1	3.7

Data were collected during resting phase and repeated three times for each muscle. As for *vastus lateralis* muscle, subjects were seated in upright position with the knee angle of 90° and hip angle of 120° (180° corresponding to full extension). As for *biceps brachii* muscle, participants were seated upright with shoulder angle at 0° and the elbow joint at 90° (180° corresponding to full extension), and with the forearm in a supinated position. Every time, about 10 minutes of rest were allowed before an acquisition of 60 s.

2.2.2. TD NIRS setup

The non-invasive TD NIRS measurements were performed with the medical device described in our previous work [24], which was customized for muscles probing. Light at two different wavelengths ($\lambda_1 = 690$ nm and $\lambda_2 = 830$ nm) was delivered to the tissue and recollected at two interoptode distances: one short ($\rho_S = 15$ mm) and one long ($\rho_L = 30$ mm). The optical fibers were hold in place by means of a 3D printed custom probe [25], which allowed easy placement and good adhesion on the limbs, avoiding movement artifacts. The backscattered signal was then processed by two Time Correlated Single Photon Counting boards and the photons DTOFs reconstructed for each sample point.

The signal was acquired at a sampling frequency of 2 Hz. Since the TD NIRS device employs a space multiplexing approach [26] for illuminating the tissue at two different wavelengths, an integration time of 250 ms was exploited to reconstruct the DTOF at each wavelength.

An IRF was acquired for each session to account for possible time drifts of the instrument [27,28]. For convenience and speed of the operation, a reflectance implementation of IRF was used, exploiting the system already presented by some of the authors [29].

For *in-vivo* measurements, the TD NIRS probe was positioned on the left leg (or arm) and an adhesive black bandage was employed to fix the probe holding the optical fibers upon the belly of the investigated muscle *i.e.*, the *vastus lateralis* in the first session and the *biceps brachii* during the second one. In this way, motion artifacts were prevented and shielding from the background light guaranteed.

2.3. DPF calculation

Both in the simulation study and in the *in-vivo* experiments, the DPF was calculated employing Eq. (2). In particular, the barycenter of the DTOF $\langle t(\lambda) \rangle$ was estimated, after background subtraction, by considering all points in the DTOF between 1% of the peak. The barycenter of the IRF was also subtracted [30] from each curve. In the *in-vivo* measurements analysis, this calculation was repeated for the DTOF acquired at every wavelength, every source-detector separation distance and for every time of acquisition of both leg and arm of each subject.

2.4. In-vivo data statistical analysis

To evaluate the dependence of the experimental DPF on the wavelength λ and the source-detector separation ρ, the set of experimental DPF values obtained for each type of muscle *i.e.*, *vastus lateralis* and *biceps brachii*, was divided into four sub-groups: (ρ_S, λ_1), (ρ_S, λ_2), (ρ_L, λ_1), (ρ_L, λ_2). For each combination of λ and ρ, the average DPF values over 60 s of rest acquisition were calculated for each subject. Considering the small size of the population, non-parametric statistical tests were then performed.

Differences among the four populations within each muscle were evaluated through the Wilcoxon signed-rank test for paired samples. A Wilcoxon rank sum test was employed to verify the differences between the values obtained for arms and legs muscles, considered as independent samples. Finally, a possible association between DPF populations and the ATT values was investigated with the calculation of the Pearson correlation coefficients and the associated p-values.

All the statistical tests were performed with 5% significance level, exploiting MATLAB (R2019b), The MathWorks, Inc.

3. Results

3.1. Analytical simulations results

In Fig. 1, the DPF values found with the simulation process against the optical properties of the first layer are reported when different ATT are simulated. The two columns of the figure show

the results obtained for DTOF simulated at $\rho_S = 15$ mm and $\rho_L = 30$ mm, respectively. In these cases, namely simulations 1 and 2 as reported in Table 1, the optical properties of the second layer are constant. At both ρ, DPF value decreases when the coefficient μ_{a0} increases (Fig. 1(a)). This variation is almost negligible if the ATT is lower than 2.5 mm, while it is accentuated for a larger ATT. Moreover, in this case the decreasing trend observed with respect to the absorption coefficient is non-linear. Only in the range of μ_{a0} between 0.15 cm^{-1} and 0.2 cm^{-1}, the DPF value appears to be less dependent on the ATT.
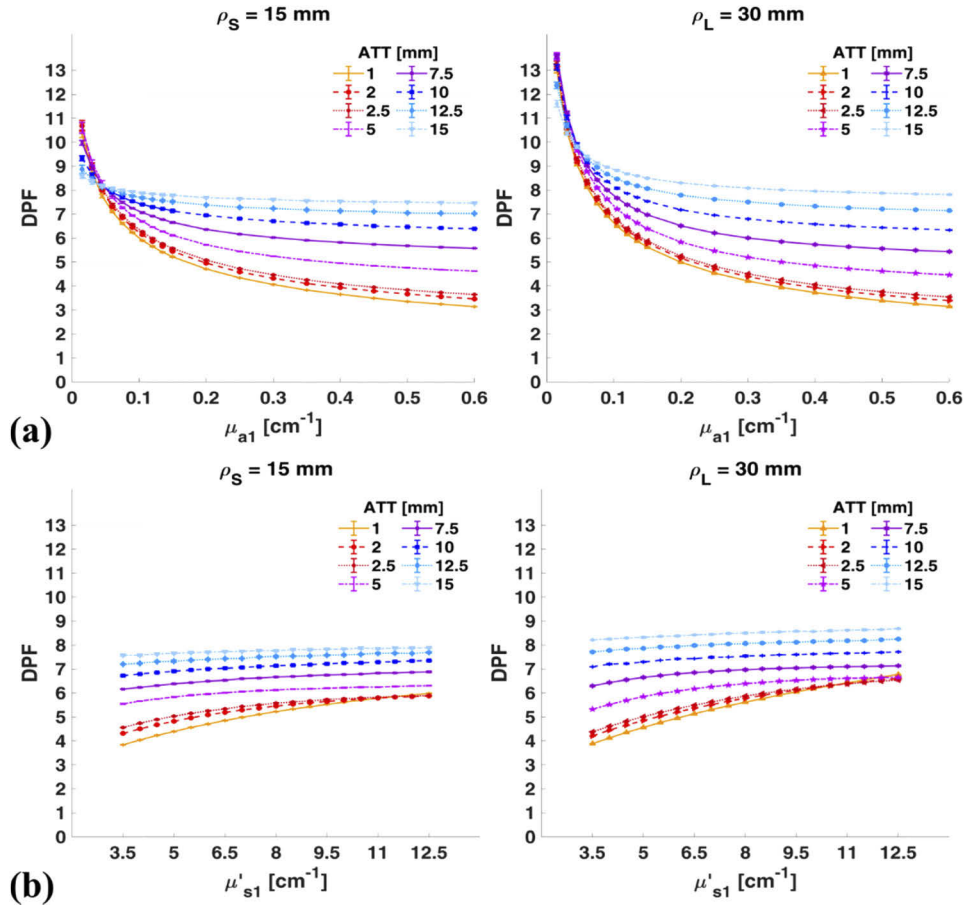

Fig. 1. DPF (dots: average of 10 values, bars: standard deviations) obtained for simulated DTOF at two source-detector distances ($\rho_S = 15$ mm and $\rho_L = 30$ mm in columns) plotted against the (a) absorption coefficient of the first layer and (b) reduced scattering coefficient of the first layer for the different values of ATT [mm].

On the other hand, looking at the relation between DPF and reduced scattering coefficient in Fig. 1(b), we noticed that the DPF increases with increasing μ'_{s0}. The trends here observed can be considered almost linear for ATT > 5 mm. Below this threshold, a non-linear behavior and a general reduced variation can be observed among the DPF values when the simulated tissue μ'_{s0} changes.

The same comparisons were performed varying the optical properties of the deep layer, while those of the superficial layer were kept constant (Simulations 3 and 4). Figure 2(a) is structured as the previous one, but in the x-axis we find the varying optical properties for the deep layer. As for the previous case, we observe that DPF values decrease when μ_{a1} increases. The trend here is

non-linear for all the considered ATT values, even though the effect becomes more accentuated for smaller (< 10 mm) ATT. Moreover, the global variation found is higher for the results at $\rho_L = 30$ mm, with a decreasing DPF range between 13.5 and 3, with respect to the results obtained at $\rho_S = 15$ mm (DPF decreasing range between 11 and 3). The ATT seems to less affect the DPF for μ_{a1} values around 0.03 cm^{-1}, where the DPF values are more similar.

Fig. 2. DPF (dot: average of 10 values, bars: standard deviations) obtained for simulated DTOF at two source-detector distances ($\rho_S = 15$ mm and $\rho_L = 30$ mm in columns) plotted against the (a) absorption coefficient of the second layer and (b) reduced scattering coefficient of the second layer for the different values of ATT [mm].

As already found in Fig. 1(b), in Fig. 2(b) DPF increases with increasing μ'_{s1}, even though the magnitude of the variation for each ATT value is here lower than the one that occurs for varying μ_{a1}, especially for ATT greater than 5 mm. For ATT < 5 mm, the non-linear trend is more accentuated, in particular for μ'_{s1} below 9 cm^{-1}.

To better highlight the relationship between the DPF and the ATT, in Fig. 3 and Fig. 4 we plot the DPF retrieved against the different ATT as a function of the varying optical properties.

In Fig. 3(a), the reduced scattering coefficient of the superficial layer is fixed ($\mu'_{s0} = 10$ cm^{-1}) and the absorption coefficient is changing. For ATT < 2.5 mm at $\rho_S = 15$ mm and ATT < 5 mm at $\rho_L = 30$ mm, the DPF is quite constant and the dependence on the μ_{a0} is less evident. For higher ATT values, a different behavior can be noticed according to the absorption coefficient. For $\mu_{a0} > 0.2$ cm^{-1}, the DPF decreases when the first layer thickness increases. For $\mu_{a0} = 0.15$
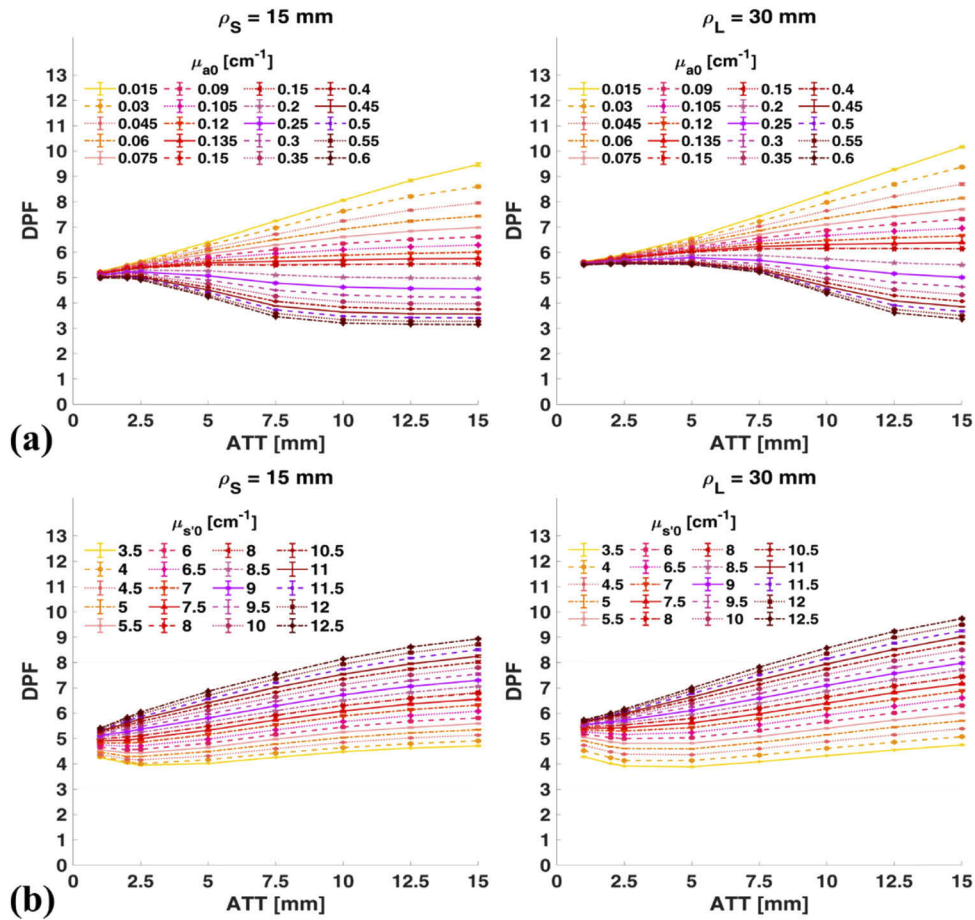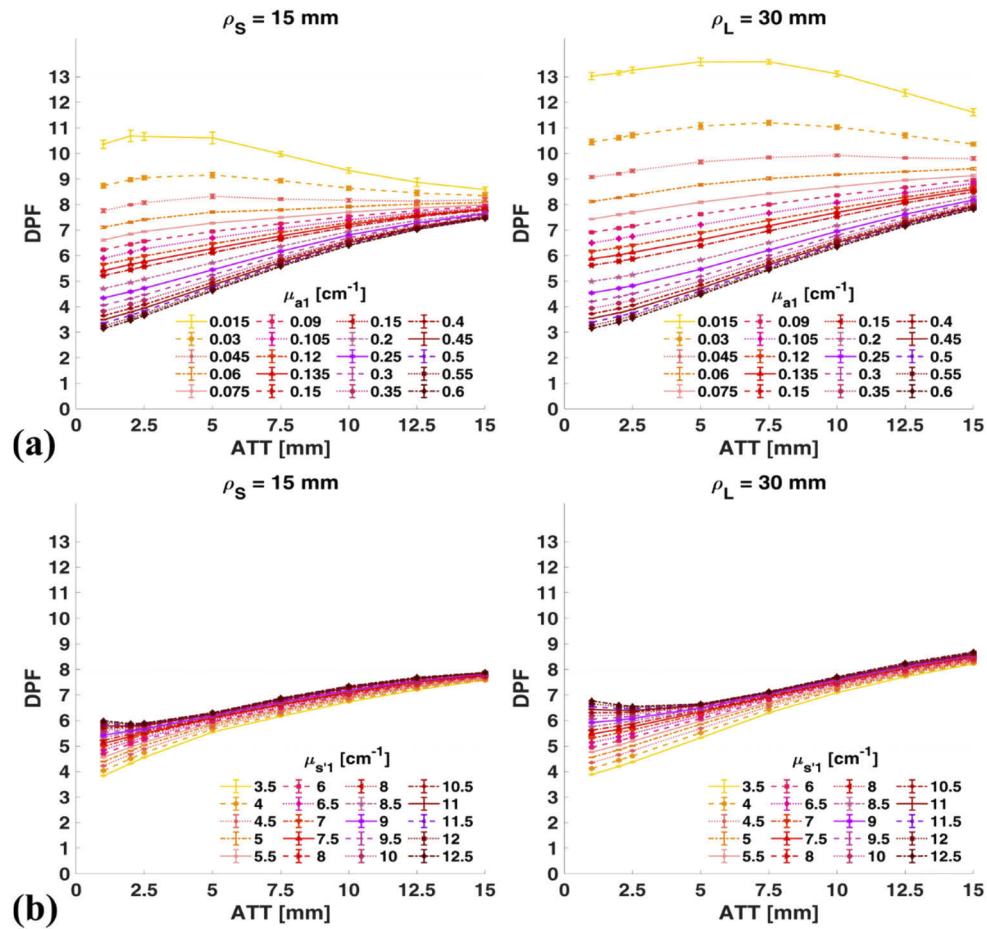
Fig. 3. DPF (dots: average of 10 values, bars: standard deviations) obtained for simulated DTOF at two source-detector distances ($\rho_S = 15$ mm and $\rho_L = 30$ mm in columns) plotted against the ATT when (a) absorption coefficient of the first layer varies ($\mu_{a0} = 0.015 - 0.6$ cm^{-1} in steps of 0.015 cm^{-1}) and (b) reduced scattering coefficient of the first layer varies ($\mu'_{s0} = 3.5 - 12.5$ cm^{-1} in steps of 0.5 cm^{-1}).

Fig. 4. DPF (dots: average of 10 values, bars: standard deviations) obtained for simulated DTOF at two source-detector distances (ρ_S = 15 mm and ρ_L = 30 mm in columns) plotted against the ATT when a) absorption coefficient of the second layer varies (μ_{a1} = 0.015 - 0.6 cm^{-1} in steps of 0.015 cm^{-1}) and b) reduced scattering coefficient of the second layer varies (μ'_{s1} = 3.5 - 12.5 cm^{-1} in steps of 0.5 cm^{-1}).

cm^{-1} the DPF is almost constant regardless of the ATT, while for $\mu_{a0} < 0.15$ cm^{-1}, the DPF increases with increasing thicknesses. In Fig. 3(b), the results of the second simulation, where the absorption of the superficial layer is fixed ($\mu_{a0} = 0.05$ cm^{-1}) and the reduced scattering coefficient is changing, are reported. In general, an increasing trend of the DPF is observed along with the ATT. However, for all the values of μ'_{s0} tested, this trend is more accentuated for ATT > 2.5 mm, while the DPF can be considered almost constant when the ATT < 2.5 mm.

In Fig. 4 the relation of DPF against ATT for the simulations 3 (Fig. 4(a)) and 4 (Fig. 4(b)) are reported. In this case, the superficial layer is constant and only the deep layer optical properties are changing. In Fig. 4(a), the trend observed is actually the opposite than the one observed in Fig. 3(a): a positive relationship between DPF and superficial layer thickness is observed for $\mu_{a1} > 0.06$ cm^{-1} and it is more accentuated as the μ_{a1} values increase. As already observed in Fig. 2(a), the ATT has less influence for $\mu_{a1} = 0.03$ cm^{-1} and the ATT < 5 mm, while a decreasing behavior can be observed for $\mu_{a1} < 0.03$ and the ATT > 5 mm. At the longer source-detector distance $\rho_L = 30$ mm, these trends are replicated, but the magnitude of DPF variations increases, in particular at low μ_{a1} (< 0.045 cm^{-1}).

In Fig. 4(b), (a) positive relation between DPF and ATT is observed regardless of the μ'_{s1} coefficient. Increasing the μ'_{s1} coefficient, the DPF increases, even though the range of variation is here lower with respect to the one observed at different absorption coefficients in Fig. 4(a).

It is worth noting that for thicknesses below 2.5 mm and μ'_{s1} higher than 9 cm^{-1}, the DPF values are almost constant. Even in this case, we observe the same behavior at the source-detector distance $\rho_L = 30$ mm, but higher differences between the retrieved values are shown for ATT < 5 mm.

3.2. In-vivo study results

DPF assessment was conducted in resting conditions, when confounding factors as movement artifacts or variations of the optical properties due to muscle contractions can be excluded. In Fig. 5, we show the boxplots for the population's DPFs values experimentally retrieved during the baseline measurements. The dots represent the average values over the first 60 s at rest for each subject. The following color coding for the wavelength/interfiber distances combination is kept in these boxplots and will be maintained for the whole section: (ρ_S, λ_1), in light blue, (ρ_S, λ_2) in blue, (ρ_L, λ_1) in red, (ρ_L, λ_2) in yellow.

A considerable variation between subjects is observed, with values ranging from 2.9 to 6.1 for legs and from 2.8 to 5.0 for arms. Moreover, a significant difference between the muscles of the same subject was found (0.02 < p-values < 0.05). In general, higher DPF values for the *vastus lateralis* muscles with respect to the *biceps brachii* ones were observed. In Table 3, the descriptive statistics indices of the populations are reported in details.

Table 3. Summary of DPF values population of vastus lateralis and biceps brachii retrieved for the 11 subjects probed during the first baseline measurement.

| DPF | Vastus Lateralis | | Biceps Brachii | |
| | $\rho_S = 15$ mm | | $\rho_L = 30$ mm | |
	$\lambda_1 = 690$ nm	$\lambda_2 = 830$ nm	$\lambda_1 = 690$ nm	$\lambda_2 = 830$ nm
Mean	4.68	4.16	3.91	3.57
Median	4.73	4.25	3.78	3.53
Std. Dev.	0.79	0.72	0.48	0.44
IQR	2.13	2.12	1.47	1.31

Moreover, looking at the sub-groups for the same type of muscle, a wavelength dependence is observed. In our data, the DPF calculated at 830 nm appears to be significantly (p < 0.001)
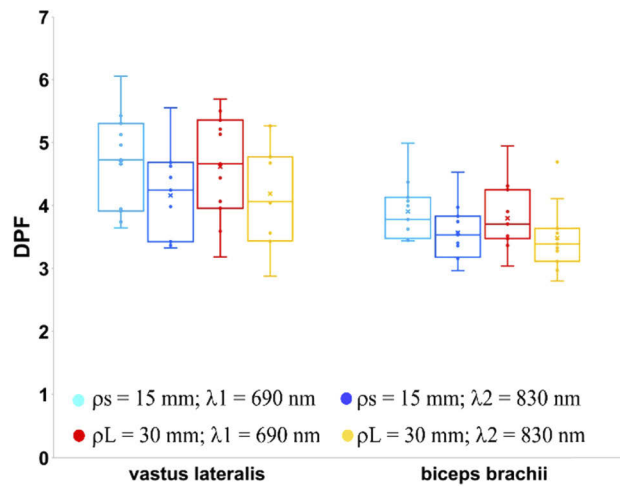
Fig. 5. Comparison between DPF calculated at rest for v*astus lateralis* (left side) and *biceps brachii* (right side) of the entire population. The values are visualized with different colors for each wavelength (λ_1 and λ_2) and source-detector separation (ρ_S and ρ_L) combination. In each boxplot, the box length represent the interquartile range (IQR), therefore lower and upper boundaries of the box represent the 25th and 75th percentile respectively; the horizontal middle line corresponds to the median value of the population and the external whiskers include data within $\pm 1.5 \times$IQR.

smaller than the one at 690 nm. On the other hand, no significant influence of source-detector separation distances on the DPFs could be observed.
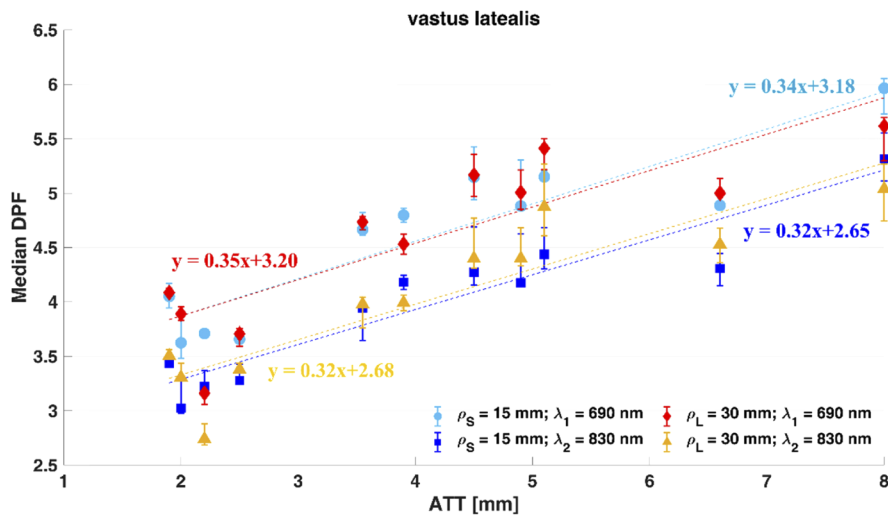

Fig. 6. *In-vivo* v*astus lateralis* DPFs vs the ATT of each subject. The DPF median values (dots) of three repeated rest measurements, lasting 60 s each, are represented separately for each wavelength (λ_1 and λ_2) and source-detector separation (ρ_S and ρ_L) combination. For each dot, the upper and lower bars represent respectively the maximum and minimum deviation from the median value. Trend lines for each series ($0.73 < R^2 < 0.88$) are superimposed.

In addition, the DPF relation with the ATT was investigated and depicted in Fig. 6 and Fig. 7. For each subject, reproducible DPF values are obtained in three repeated rest measurements. For both arms and legs, a difference of 0.2 ± 0.2 (mean $\pm$ SD) was found among values.
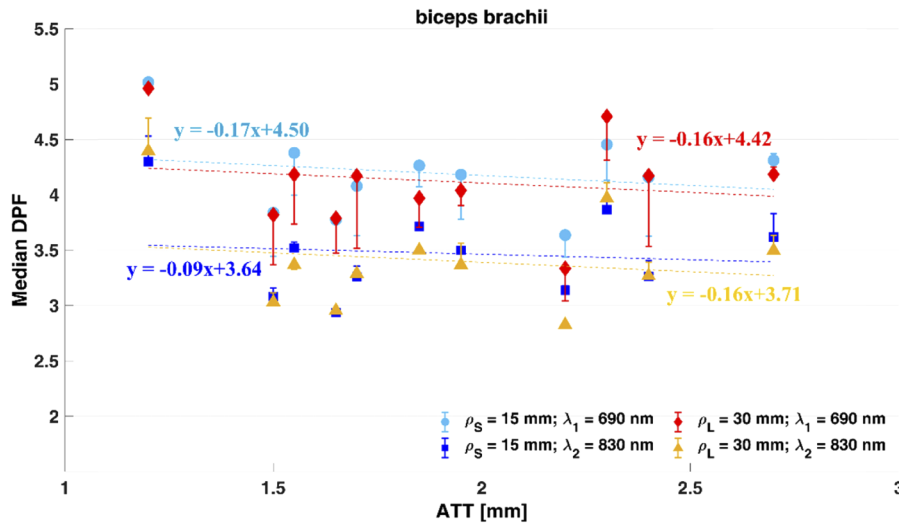

Fig. 7. *In-vivo biceps brachii* DPFs vs the ATT of each subject. The DPF median values (dots) of three repeated rest measurements, lasting 60 s each, are represented separately for each wavelength (λ_1 and λ_2) and source-detector separation (ρ_S and ρ_L) combination. For each dot, the upper and lower bars represent respectively the maximum and minimum deviation from the median. Trend lines for each series ($0.01 < R^2 < 0.05$) are superimposed.

Focusing on the measurements of the *vastus lateralis* in Fig. 6, where the ATT ranges from 1.9 to 8 mm, a positive correlation between the DPF and the subcutaneous thickness can be observed at all wavelengths and interfiber distances ($0.85 < R < 0.94$ and p-value < 0.001). This relationship is also well represented by linear trend lines, whose equations have positive 1st order coefficients.

This dependence is not significant for the *biceps brachii* muscles in Fig. 7, where the thickness range is reduced (from 1.2 to 2.3 mm) and Pearson coefficients R of -0.1 were found for each sub-group. Also, the 1st order coefficients of the trend lines reported in Fig. 7 are close to zero for all the series.

4. Discussion

The present work addresses with a systematic approach the study of the DPF in the skeletal muscle and how its value can be affected by changes in tissue optical properties, wavelength, source-detector distance and ATT.

From the simulations, we can observe that changes of optical properties either in the superficial layer, or in the muscle layer, do influence the DPFs absolute values. In general, when the absorption coefficient of either the superficial or the deep layer increases, the DPF tends to decrease. In fact, since the photons are easily absorbed, their path into the tissue is shortened and this characteristic is accounted by a smaller DPF value. On the contrary, when the reduced scattering coefficient of one of the two layers increases, it means that the path travelled by the photons inside the tissue is extended due to the several scattering events, and the DPF increases as well. Similar results have been already reported by Gao *et al* [11]. for head measurements.

In addition, we found that the magnitude of the DPF variations depends on the thickness of the first layer encountered by the photons *i.e.*, the ATT. In 1996, Homma *et al.* [31] observed a

variation of light propagation and of the measured optical density for different ATT in muscles. They performed measurements of the *extensor hallucis longus* muscle and of the *extensor digitorum longus* muscle of eleven subjects with a CW NIRS device. They found that only when the ATT was thin and the source-detector distance was below 40 mm, the light could penetrate the limb enough to reach the muscle.

In 2003, Wolf *et al.* [21] reported measurements on the human calf muscle with a FD NIRS instrumentation. The absorption and the reduced scattering coefficients were estimated in different location of the *later gastrocnemius* muscle, exploiting different interoptode distances and a homogeneous medium model. They observed a constant μ'_s and decreasing μ_a with increasing ATT.

In our study, where a bilayer model of the medium was assumed, we found that when the ATT is small (below 2.5 mm), the DPF seems to be mainly affected by the variation of the optical properties of the deep layer. In particular, in case of high scattering and low absorption properties, the DPF trend is almost constant. For larger values of the ATT, the optical properties of the superficial layer progressively influence the DPF.

The ATT and the tissue optical properties also influence the relation between the DPF values and the source-detector separation. In fact, from the simulations, we can say that the chosen interfiber distance has a greater impact on the DPF of the whole tissue in two cases: when the subcutaneous layer is thick and its optical properties are changing or when the superficial layer is thin and only the deeper layer properties are varying.

Finally, we observed that variations of the absorption coefficients are related to changing of DPF in a non-linear way, even if the reduced scattering coefficient is kept constant. The non-linear decreasing trend can have different slope according to the magnitude of the absorption variation and the ATT. Actually, we observed only a small range of absorption coefficient (0.15 cm^{-1} $< \mu_{a0} < 0.2$ cm^{-1} and $\mu_{a1} = 0.03$ cm^{-1}) when the influence of ATT can be considered negligible.

During *in-vivo* measurements, data acquisition was performed on upper and lower limbs in order to assess potential effects of changes in both superficial (different ATT) and deep layer (different muscles) optical properties. The resulting effect on the DPF value is the combination of these two factors.

In particular, looking at the plot of the DPF against the ATT obtained for *vastus lateralis* in resting conditions (Fig. 6), we observe an increasing trend. It corresponds to the trend found in the same plots for the simulated curves (Fig. 3(a) and Fig. 4(a)), when $\mu_{a0} < 0.15$ cm^{-1}, $\mu_{a1} > 0.45$ cm^{-1} and the ATT is larger than 2 mm. In fact, this scenario resembles the one we measured for the legs, where we found a thicker (always > 2 mm) first adipose layer, less absorbing then the muscle in the second layer at the wavelengths employed. Aiming at comparing with simulated data and with previously published data, in the *in-vivo* assessment we performed an estimation of the leg optical properties (μ_a and μ'_s) employing a photon diffusion model for a semi-infinite homogeneous medium. At $\rho_L = 30$ mm, μ_a was equal to 0.25 ± 0.07 cm^{-1} (0.28 ± 0.08 cm^{-1}) 690 nm (830 nm) and μ'_s to 8.14 ± 1.44 cm^{-1} (7.15 ± 1.40 cm^{-1}) at 690 nm (830 nm). At $\rho_s = 15$ mm, μ_a equal to 0.22 ± 0.08 cm^{-1} (0.24 ± 0.08 cm^{-1}) 690 nm (830 nm) and μ'_s to 8.84 ± 0.80 cm^{-1} (7.14 ± 0.82 cm^{-1}) at 690 nm (830 nm) were estimated. Furthermore, we compared the DPF estimated by Eq. (3), based on the found optical properties, with respect to the values calculated by Eq. (2), exploiting the average photons time-of-flight. At $\rho_L = 30$ mm, we found an average relative percentage difference of $5.74 \pm 4.05\%$ ($5.76 \pm 3.35\%$) at 690 nm (830 nm). At $\rho_s = 15$ mm, a relative percentage difference of $5.85 \pm 4.36\%$ ($6.56 \pm 4.66\%$) at 690 nm (830 nm) was calculated. A significant difference between the DPF values obtained with the two different approaches was observed only at $\rho_s = 15$ mm and 690 nm (Wilcoxon signed-rank test, p-value $= 0.02$). Since a large variation of DPF difference values among the legs population was found, a larger sample for each ATT value could lead at different results.

The same correlation between DPF and ATT is not evident from the experimental data acquired on the *biceps brachii*. This difference between arms and legs populations can be explained by the small range of variation of the ATT observed in the arms of the recruited subjects (1.2 mm < ATT < 2.3 mm). In fact, when the ATT range is so small, the DPF can be considered constant even in the simulations.

As for the optical properties estimated with a homogeneous medium model, at $\rho_L = 30$ mm, $\mu_a = 0.27 \pm 0.05$ cm^{-1} (0.34 ± 0.05 cm^{-1}) at 690 nm (830 nm) and $\mu'_s = 7.27 \pm 1.34$ cm^{-1} (6.44 ± 1.35 cm^{-1}) at 690 nm (830 nm) were found. At $\rho_s = 15$ mm, μ_a equal to 0.25 ± 0.05 cm^{-1} (0.30 ± 0.06 cm^{-1}) 690 nm (830 nm) and μ'_s to 8.09 ± 1.18 cm^{-1} (6.78 ± 0.93 cm^{-1}) at 690 nm (830 nm) were estimated. The relative differences between the DPF estimated with Eq. (3) with respect to Eq. (2) were equal to $2.74 \pm 0.63\%$ ($3.35 \pm 0.96\%$) at 690 nm (830 nm) and $\rho_L = 30$ mm. At $\rho_s = 15$ mm, the difference was equal to $5.51 \pm 1.27\%$ ($7.27 \pm 1.60\%$) at 690 nm (830 nm). A significant difference was found (Wilcoxon signed-rank test, p-value < 0.001) among all the populations of *biceps brachii* DPF. These differences can be due to the fact that the values derived from Eq. (2) do not rely on any physics models for photons propagation, in contrast to Eq. (3) based on a homogeneous tissue model.

Moreover, in our *in-vivo* data, we found a dependence of the DPF on the wavelength, lower values could be observed at greater wavelength. This tendency is in accordance with data reported in literature. In fact, the wavelength dependence of the DPF for the head, the forearm and the calf muscles has already been shown by Essenpreis *et al* [8]. According to their results, a general reduction of the DPF in the near infrared spectral range, especially beyond 800 nm, can be explained by an increased absorption of the main chromophores *i.e.*, the oxy- and [deoxy(Hb + Mb)]. This effect is accentuated by a decreased reduced scattering coefficient of the tissue, accordingly to the Mie scattering theory [32].

In the same framework, Kohl *et al.* [14] proposed a technique to derive the wavelength dependence of the DPF of the head from measurements of pulse-induced attenuation changes. They found a monotonically decreasing relationship between 700 nm and 1000 nm.

On the other hand, the relationship between DPF values and the source-detector separation distance is not straightforward. In the simulations, performed considering the same distances ρ_S and ρ_L employed in the *in-vivo* study, this relationship depends on the ATT and the tissue optical properties whereas optical properties of both layers simultaneously changed in the experimental measurements. It should be noted that the range of variation of the ATT in the legs goes from 1.9 mm up to 8 mm and these differences may act as confounding factor. Thus, the average of the whole population (Fig. 5) may not show a clear influence of the source-detector distance on the DPF values retrieved. Nevertheless, it is clear from the boxplots represented that, besides an inter-muscle variability, there is a considerable inter-subjects variability.

Considering the key role of DPF, according to Eq. (1), in retrieving the variations of [deoxy(Hb + Mb)] and [oxy(Hb + Mb)] concentrations, it is suggested that its accurate and actual determination is crucial. The approach frequently employed in single distance CW NIRS methods, where a single common DPF value is taken and applied for all the subjects, can lead to inaccurate absolute values of the hemoglobin and myoglobin concentrations.

Since the DPF is intrinsically related to the absorption and the reduced scattering coefficients, even when applying approaches that tries to overcome the DPF specific determination *e.g.*, the multi-distance approaches or the so-called spatially resolved spectroscopy [6], we strongly suggest caution in the usage of fixed values of optical properties given by literature.

Moreover, based on the non-linear behavior observed for the DPF in simulated situations when the optical properties change, we can suppose that even the DPF of the same limb can dynamically change over time. This is the case, for example, during exercise, when the absorption and reduced scattering coefficients of the muscles change due to variation of the oxygen consumption and structure organization of the tissue itself [13]. Actually, Barstow *et al.* already reported in

literature that the muscle DPF can change over time during the exercise [33]. Further investigation of the actual impact of the DPF variation during exercise on the Hb and Mb concentration retrieved by CW NIRS would be required. In this direction, Ferreira *et al.* [34] investigated the influence of assuming a constant optical scattering on measurements of *vastus lateralis* oxygenation during an incremental cycling exercise. In this work, the authors exploited a FD NIRS system to retrieve time-dependent μ_a and μ'_s and dynamically calculated the DPF using a simplified version of Eq. (3). They found that a constant μ'_s led to an overestimation of variation of both [deoxy(Hb + Mb)] and [oxy(Hb + Mb)], and an alteration of their time-course. The employment of a time-dependent DPF seems to be a preferable choice to obtain accurate results.

Even though the panorama of combinations of the parameters explored with our simulation study can cover different scenarios of *in-vivo* optical properties and their variations, further experimental studies should be carried out. More subjects should be enrolled, taking into consideration different types of muscles, subcutaneous ATTs and exercise conditions in order to evaluate to which extend the DPF values are influenced by these factors during dynamic experiments. Furthermore, extending the subjects' recruitment criteria *e.g.*, including also females and increasing the age range, would provide a reliable database of DPF values, investigating the possible influence of sex and aging, as it was done in some cerebral, calf and forearm studies [12,23]. This would also lead to the possibility of defining a new equation, similarly to Eq. (3), by which the relationship between the DPF and all the mentioned factors, starting with the ATT, could be expressed for a layered medium.

5. Conclusions

In this paper, we show that ATT, tissue optical properties, source detector distances and wavelengths can affect DPF estimation for NIRS skeletal muscles measurements. From systematic simulations, we observe that the DPF value is affected by the optical properties of both the subcutaneous adipose tissue and the deeper skeletal muscle at thicker ATTs. Furthermore, the peculiar optical properties of the tissues can affect the weight of the different layers in the result DPF value, especially if the properties change. TD NIRS *in-vivo* measurements conducted at rest on two skeletal muscles (*vastus lateralis* and *biceps brachii)* confirmed relations among the DPF, the absorption and reduced scattering coefficients and the ATT. Even though the population of subjects enrolled in this study was quite homogeneous, all males about the same age and in comparable physical conditions, DPF differences were found among each subject and even among different muscles. These results suggest that a personalized time-dependent DPF should be calculated and considered for a correct estimation of the oxy- and [deoxy(Hb + Mb)]. Nowadays, the employment of NIRS technique is becoming widespread in a scenario of multimodal non-invasive measurements. Indeed, several research studies has demonstrated the utility of NIRS parameters in both clinical populations, as diagnostic or rehabilitation monitoring tool, and healthy subjects for the evaluation of physical performance [3,35]. For this reason, the quantitative and correct evaluation of muscle oxidative metabolism changes is crucial and it requires the accurate knowledge, specific for each subject and tissue investigated, of all the parameters, including the DPF, concurring to their definition.

Disclosures. D.C. and A.T.: pioNIRS S.r.l., Italy (I). Other authors declare no conflicts of interest related to this article.

References

1. R. Boushel and C. A. Piantadosi, "Near-infrared spectroscopy for monitoring muscle oxygenation," Acta Physiol. Scand. **168**(4), 615–622 (2000).

2. S. Jones, S. T. Chiesa, N. Chaturvedi, and A. D. Hughes, "Recent developments in near-infrared spectroscopy (NIRS) for the assessment of local skeletal muscle microvascular function and capacity to utilise oxygen," Artery Res. **16**(C), 25–33 (2016).

3. B. Grassi and V. Quaresima, "Near-infrared spectroscopy and skeletal muscle oxidative function *in vivo* in health and disease: a review from an exercise physiology perspective," J. Biomed. Opt. **21**(9), 091313 (2016).

4. M. D. Campbell and D. J. Marcinek, "Evaluation of in vivo mitochondrial bioenergetics in skeletal muscle using NMR and optical methods," Biochim. Biophys. Acta **1862**(4), 716–724 (2016).

5. B. Zeller-Plumhoff, T. Roose, G. F. Clough, and P. Schneider, "Image-based modelling of skeletal muscle oxygenation," J. R. Soc. Interface **14**(127), 20160992 (2017).

6. F. Scholkmann, A. J. Metz, and M. Wolf, "Measuring tissue hemodynamics and oxygenation by continuous-wave functional near-infrared spectroscopy - How robust are the different calculation methods against movement artifacts?" Physiol. Meas. **35**(4), 717–734 (2014).

7. F. Scholkmann, S. Kleiser, A. J. Metz, R. Zimmermann, J. Mata Pavia, U. Wolf, and M. Wolf, "A review on continuous wave functional near-infrared spectroscopy and imaging instrumentation and methodology," Neuroimage **85**, 6–27 (2014).

8. M. Essenpreis, M. Cope, C. E. Elwell, S. R. Arridge, P. van der Zee, and D. T. Delpy, "Wavelength depencence of the differential pathlength factor and the log slope in time-resolved tissue spectroscopy," in *Optical Imaging of Brain Function and Metabolism*, P. U. Dirnagl, A. Villringer, and K. M. Einhäupl, eds. (Springer Science + Business Media, 1993), p. 9.20.

9. F. Scholkmann, H. Zohdi, N. Nasseri, and U. Wolf, "Absolute values of optical properties (μa, μ's, μeff and DPF) of human head tissue: Dependence on head region and individual," Adv. Exp. Med. Biol. **1072**, 325–330 (2018).

10. M. A. Kamran, M. M. Naeem Mannan, and M. Y. Jeong, "Initial-dip existence and estimation in relation to DPF and data drift," Front. Neuroinform. **12**, 1–13 (2018).

11. L. Gao, C. E. Elwell, M. Kohl-Bareis, M. Gramer, C. E. Cooper, T. S. Leung, and I. Tachtsidis, "Effects of assuming constant optical scattering on haemoglobin concentration measurements using NIRS during a Valsalva manoeuvre," Adv. Exp. Med. Biol. **701**, 15–20 (2011).

12. A. Duncan, J. H. Meek, M. Clemence, C. E. Elwell, L. Tyszczuk, M. Cope, and D. Delpy, "Optical pathlength measurements on adult head, calf and forearm and the head of the newborn infant using phase resolved optical spectroscopy," Phys. Med. Biol. **40**(2), 295–304 (1995).

13. M. Ferrari, Q. Wei, R. A. De Blasi, V. Quaresima, and G. Zaccanti, "Variability of human brain and muscle optical pathlength in different experimental conditions," in *Photon Migration and Imaging in Random Media and Tissues*, B. Chance and R. R. Alfano, eds. (SPIE, 1993), 1888, pp. 466–472.

14. M. Kohl, C. Nolte, H. R. Heekeren, S. Horst, U. Scholz, H. Obrig, and A. Villringer, "Determination of the wavelength dependence of the differential pathlength factor from near-infrared pulse signals," Phys. Med. Biol. **43**(6), 1771–1782 (1998).

15. A. M. Chiarelli, D. Perpetuini, C. Filippini, D. Cardone, and A. Merla, "Differential pathlength factor in continuous wave functional near-infrared spectroscopy: reducing hemoglobin's cross talk in high-density recordings," Neurophotonics **6**(03), 1 (2019).

16. D. Piao, R. L. Barbour, H. L. Graber, and D. C. Lee, "On the geometry dependence of differential pathlength factor for near-infrared spectroscopy. I. Steady-state with homogeneous medium," J. Biomed. Opt. **20**(10), 105005 (2015).

17. K. Tsukahara, Y. Takema, S. Moriwaki, T. Fujimura, and G. Imokawa, "Dermal fluid translocation is an important determinant of the diurnal variation in human skin thickness," Br. J. Dermatol. **145**(4), 590–596 (2001).

18. F. Martelli, A. Sassaroli, Y. Yamada, and G. Zaccanti, "Analytical approximate solutions of the time-domain diffusion equation in layered slabs," J. Opt. Soc. Am. A **19**(1), 71–80 (2002).

19. P. Tothill and A. D. Stewart, "Estimation of thigh muscle and adipose tissue volume using magnetic resonance imaging and anthropometry," J. Sports Sci. **20**(7), 563–576 (2002).

20. N. Nasseri, S. Kleiser, D. Ostojic, T. Karen, and M. Wolf, "Quantifying the effect of adipose tissue in muscle oximetry by near infrared spectroscopy," Biomed. Opt. Express **7**(11), 4605 (2016).

21. U. Wolf, M. Wolf, J. H. Choi, L. A. Paunescu, L. P. Safonova, A. Michalos, and E. Gratton, "Mapping of hemodynamics on the human calf with near infrared spectroscopy and the influence of the adipose tissue thickness," Adv. Exp. Med. Biol. **510**, 225–230 (2003).

22. F. Martelli, S. Del Bianco, A. Ismaelli, and G. Zaccanti, *Light Propagation through Biological Tissue and Other Diffusive Media: Theory, Solutions, and Software* (SPIE, 2010).

23. F. Scholkmann and M. Wolf, "General equation for the differential pathlength factor of the frontal human head depending on wavelength and age," J. Biomed. Opt. **18**(10), 105004 (2013).

24. R. Re, I. Pirovano, D. Contini, L. Spinelli, and A. Torricelli, "Time Domain Near Infrared Spectroscopy Device for Monitoring Muscle Oxidative Metabolism: Custom Probe and In Vivo Applications," Sensors **18**(1), 264 (2018).

25. C. Amendola, I. Pirovano, M. Lacerenza, D. Contini, L. Spinelli, R. Cubeddu, A. Torricelli, and R. Re, "Use of 3D Printed PLA for Diffuse Optics," in *Biophotonics Congress: Biomedical Optics 2020 (Translational, Microscopy, OCT, OTS, BRAIN)* (Optical Society of America, 2020), p. JTh2A.16.

26. R. Re, D. Contini, M. Caffini, R. Cubeddu, L. Spinelli, and A. Torricelli, "A compact time-resolved system for near infrared spectroscopy based on wavelength space multiplexing," Rev. Sci. Instrum. **81**(11), 113101 (2010).

27. A. Torricelli, D. Contini, A. Pifferi, M. Caffini, R. Re, L. Zucchelli, and L. Spinelli, "Time domain functional NIRS imaging for human brain mapping," Neuroimage **85**, 28–50 (2014).

28. V. Ntziachristos and B. Chance, "Accuracy limits in the determination of absolute optical properties using time-resolved NIR spectroscopy," Med. Phys. **28**(6), 1115–1124 (2001).

29. I. Pirovano, R. Re, D. Contini, L. Spinelli, and A. Torricelli, "Instrument response function acquisition in reflectance geometry for time-resolved diffuse optical measurements," Biomed. Opt. Express **11**(1), 240–250 (2020).

30. H. Wabnitz, D. Contini, L. Spinelli, A. Torricelli, and A. Liebert, "Depth-selective analysis in time-domain optical brain imaging: moments vs time windows," Biomed. Opt. Express **11**(8), 4224–4243 (2020).

31. S. Homma, T. Fukunaga, and A. Kagaya, "Influence of adipose tissue thickness on near infrared spectroscopic signals in the measurement of human muscle," J. Biomed. Opt. **1**(4), 418–424 (1996).

32. P. Taroni, A. Pifferi, A. Torricelli, D. Comelli, and R. Cubeddu, "In vivo absorption and scattering spectroscopy of biological tissues," Photochem. Photobiol. Sci. **2**(2), 124–129 (2003).

33. T. J. Barstow, "Understanding near infrared spectroscopy (NIRS) and its application to skeletal muscle research," J. Appl. Physiol. **126**(5), 1360–1376 (2019).

34. L. F. Ferreira, D. M. Hueber, and T. J. Barstow, "Effects of assuming constant optical scattering on measurements of muscle oxygenation by near-infrared spectroscopy during exercise," J. Appl. Physiol. **102**(1), 358–367 (2007).

35. S. Perrey and M. Ferrari, "Muscle oximetry in sports science: a systematic review," Sport. Med. **48**(3), 597–616 (2018).